Plasmon-Induced Enhancement

DOI: 10.1002/anie.201002173

Silver Nanoparticle Induced Photocurrent Enhancement at WO_3 Photoanodes**

*Renata Solarska, Agata Królikowska, and Jan Augustyński**

The use of plasmonic metallic nanostructures (Ns), typically silver or gold, to enhance optical absorption in photovoltaic (PV) cells, first proposed 15 years ago,[1,2] recently received renewed attention. Surface plasmons are collective oscillations of the conduction electrons excited when metal Ns are illuminated with electromagnetic radiation. This radiation induces strong localized electromagnetic fields and leads to greatly enhanced optical absorption and scattering occurring at specific wavelengths which depend on the size and shape of the metal features.[3,4]

As a result of significantly improved light trapping, substantial gains in solar conversion efficiencies have been achieved in various PV cells including plasmonic Ns,[5] such as thin-film crystalline silicon solar cells,[6] amorphous silicon cells,[7] and organic polymer based bulk-heterojunction PV cells.[8–11] However, experiments performed with the organic PV cells also revealed enhanced charge recombination occurring at the interface between metal nanoparticles (NPs), deposited on the transparent conducting oxide (TCO) substrate, and the active layer of the solar cell. This problem could be circumvented in part by intercalating buffer layers between the plasmon-active silver islands and the exciton-generating bulk-heterojunction active layers.[8–10] It has to be noted, however, that although the employed buffer layer reduces the charge recombination, it simultaneously decreases the plasmon-enhanced absorption of the active layer of the solar cell owing to the decaying electromagnetic field with the increasing distance.

Interestingly, the use of silver plasmonic NPs was also recently reported in the case of a photoelectrochemical device, namely, a dye-sensitized solar cell, in an attempt to increase the dye extinction.[12] Silver NPs were coated with a thin protective layer of titanium dioxide to preserve them from the corrosive action of the I^-/I_3^- electrolyte. Plasmon-enhanced light absorption by the dye, consistently with a significant increase in incident photon-to-current conversion efficiencies (IPCEs), was conclusively demonstrated for the cells including silver NPs.

That work also showed the importance of the distance separating the plasmonic particles from the dye, as the measured IPCEs decreased with increasing the intensity decay of the electromagnetic field with distance.

In the present study, we investigated the suitability of plasmon-active silver NPs to enhance photocurrents associated with the photooxidation of water, generated by mesoporous tungsten trioxide (WO_3) photoanodes irradiated with visible light in aqueous solutions. Like some other large-band-gap n-type semiconducting oxides characterized by an indirect optical transition, WO_3 exhibits low absorption coefficients near the fundamental band edge which increase only quite slowly at shorter wavelengths.[13,14] In the case of WO_3 with monoclinic structure having a band gap of 2.5 eV, the long optical pathways correspond to visible wavelengths (400–500 nm), which determine the extent of solar light absorption by the photoanode material.[15] Consequently, the effective absorption by WO_3 of the visible wavelengths requires the use of thick films, which in turn increases energy losses by charge recombination and ohmic drops.

The configuration chosen for the WO_3 film photoanode including plasmonic Ns should, at first, preserve silver particles from the corrosion by the acidic electrolyte used in the photoelectrochemical cell. Another critical issue is related to the sol–gel preparation method of the films, which requires final annealing in oxygen at around 500 °C to obtain highly crystalline, photoactive n-type WO_3.[16,17] Such treatment might eventually be expected to cause oxidation of predeposited silver NPs. Preliminary experiments showed that spreading colloidal precursor solution used for the deposition of mesoporous WO_3 onto conducting glass (TCO) substrate bearing a film of silver islands actually prevented oxidation of the silver particles during the high-temperature annealing. We ascribe this effect to the presence in the precursor solution of a large amount of an organic structure-directing agent, polyethylene glycol (PEG), which undergoes progressive oxidation over a large range of temperatures with the definite elimination of organic residues occurring only at approximately 450 °C.[16]

Repetitive photoelectrochemical experiments showed also that, despite its mesoporous structure, the WO_3 film was able to preserve silver NPs against etching by the electrolyte. In fact, stable photoanodic currents were observed during prolonged measurements carried out with AgNP/WO_3 films in solutions of H_2SO_4, methanesulfonic acid, and NaCl (acidified to pH 2). The latter solution, which produced oxygen and approximately 20% chlorine at the WO_3 photoanode,[17] was chosen for its ability to form an

[*] Dr. R. Solarska, Dr. A. Królikowska, Prof. J. Augustyński
Department of Chemistry, Warsaw University
Pasteura 1, 02-093 Warsaw (Poland)
Fax: (+48) 22-822-5996
E-mail: jan.augustynski@unige.ch

[**] Financial support from NanoPEC (EU project no 227179) and a Homing Grant (Foundation for Polish Science, HOM/2009/12A,B) for R.S. is acknowledged. R.S. gratefully acknowledges Krzysztof Bieńkowski from ITME (Institute of Electronic Materials Technology, Warsaw) for SEM observations and discussion. We thank Dr. Bruce Alexander (University of Greenwich) for helpful comments and suggestions.

Supporting information for this article is available on the WWW under http://dx.doi.org/10.1002/anie.201002173.

AgCl protective layer on the surface of silver NPs. However, further experiments in which the silver NPs were first covered with a thin AgCl film formed by a short-pulse anodic oxidation in acidic NaCl solution, before depositing the WO_3 film, showed that such a pretreatment, leading to the formation of a kind of buffer layer, was not necessary. In fact, although photocurrent enhancement was still observed, it was decreased by the presence of the AgCl interlayer.

To find the optimum thickness of the silver NP layer that does not absorb too much light when the AgNP/WO_3 film is irradiated through the TCO substrate, but still assures significant enhancement of the photocurrent, nanoparticulate films corresponding to silver mass thicknesses of 2, 3, and 4 nm were compared. Extinction spectra of these three films (Figure 1 A) exhibit several maxima attributable to multiple reflections (interference fringes) observed in weakly absorbing films.[18] Generally, the extinction increases concomitantly with the film thickness.

The observed shifts in positions of the maxima in the extinction spectra shown in Figure 1 A with film thickness are apparently due to the varying shape and size of the Ag islands.

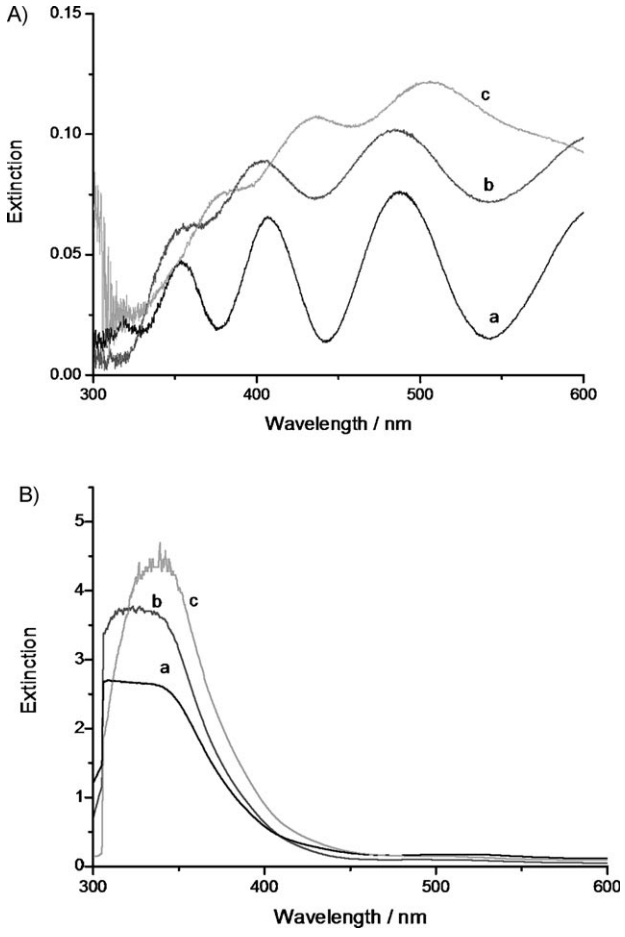

Figure 1. Extinction spectra collected for A) a series of silver films of different mass thicknesses deposited onto the TCO substrate (a: 2 nm thick Ag mass layer vs. TCO; b: 3 nm Ag; c: 4 nm Ag) and B) for 1 μm thick WO_3 films formed either onto nanoparticulate Ag layers or directly onto the TCO substrate (a: WO_3 vs. TCO; b: 3 nm Ag/WO_3 vs. TCO; c: 4 nm Ag/WO_3 vs. TCO). All spectra were recorded versus a TCO plate.

Scanning electron microscopy and atomic force microscopy images represented in Figure 2 and Figures S1 and S2 (in the Supporting Information) show that, in particular, thicker

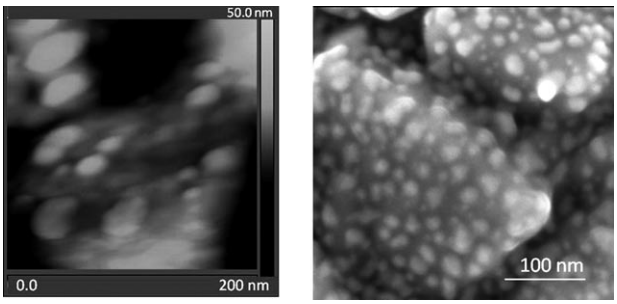

Figure 2. TM-AFM and SEM images of silver islands as a part of 3 nm thick Ag film sputtered onto the TCO substrate.

films consist of larger and more elongated NPs. Features of 10 and 17 nm mean average diameter were found for 2 and 3 nm thick silver films, respectively. Both SEM and AFM images of the 4 nm thick film (see Figures S1 c and S2 b) also indicate considerable dispersion of shapes and sizes of the Ag NPs.

As shown in Figure 1 B, the presence of the silver NP underlayer actually results in enhanced light absorption by the 1 μm thick mesoporous semiconducting WO_3 film. The largest red shift of the extinction occurs for the WO_3 photoanodes deposited onto the TCO/Ag substrates corresponding to silver thicknesses of 4 and 3 nm.

Consistent with the increased optical absorption, the silver film with 4 nm mass thickness produced larger enhancement of the photoanodic currents than the 2 or 3 nm thick Ag films. To examine photoelectrochemical properties of the photoanodes featuring silver NPs, two different cell configurations were employed in which the photoactive WO_3 layer was irradiated either from the front side (i.e., the side of the WO_3/solution interface) or from the back side (i.e., through the TCO substrate). The IPCE plots for the WO_3 films deposited directly onto the TCO substrate are compared in Figure 3 with those for the AgNP/WO_3 films including silver underlayer corresponding to 4 nm mass thickness. Both back-side and front-side irradiation of the latter photoanodes produced the IPCEs significantly (up to 50%) greater than those for the photoanodes without silver. It is significant that the larger IPCE enhancement was observed for the AgNP/WO_3 photoanode irradiated with short wavelengths from the back side (see inset of Figure 3 B). Given their short optical penetration depth within WO_3, these wavelengths are mainly absorbed in the portion of the photoactive semiconductor film close to the TCO/AgNP substrate, which remains within the range of the electromagnetic field generated by irradiated silver particles. As long as the IPCEs shown in Figure 3 were not corrected for the light absorption within the TCO substrate, the actual enhancement corresponding to the back-side irradiation of the AgNP/WO_3 photoanode was even larger. As also shown in Figure 3, a less pronounced photocurrent enhancement was still observed in the case of the front-side irradiation of the AgNP/WO_3 photoanode. We assign the latter effect to the

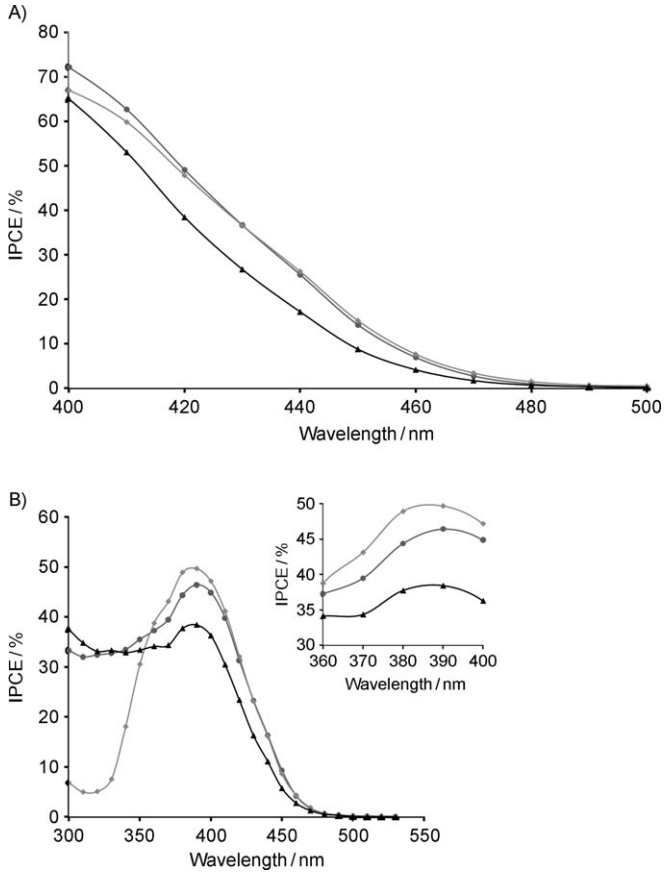

Figure 3. Incident photon to current conversion efficiency vs. wavelength plots for ca. 1 μm thick WO_3 films deposited onto 4 nm thick Ag layer (●) or directly onto the TCO substrate (▲), recorded in A) 1 M H_2SO_4 and B) 0.5 M NaCl (acidified). The electrodes were illuminated either from the WO_3/solution side (●, ▲) or through the TCO substrate (◆) at an applied potential of 1.5 V vs. the reversible hydrogen electrode (RHE). The inset shows expanded near-UV region of the IPCE spectra from Figure 3 B.

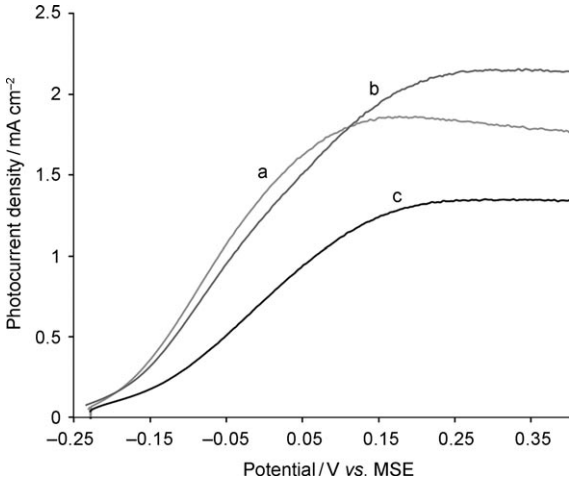

Figure 4. Photocurrent–voltage plots for ca. 1 μm thick WO_3 films deposited either onto 4 nm thick Ag underlayer (curves a and b) or directly onto the TCO substrate (curve c). The photoanodes were irradiated in a 1 M H_2SO_4 solution with simulated solar AM1.5 light either from the WO_3/solution side (curves a and c) or through the TCO substrate (curve b).

combined reflection and scattering of the incident light by the densely packed underlying silver islands (see Figure S1 c).

From the IPCE spectra, we expected a similar improvement for the photocurrents generated by the AgNP/WO_3 photoanodes under simulated air-mass (AM) 1.5 solar irradiation. Actually, the observed photocurrent enhancement was larger than that occurring under low-intensity incident light passing through the monochromator. Under the back side AM1.5 solar illumination, the photocurrent–voltage curves recorded for the photoanode featuring AgNP layer, corresponding to silver mass thickness of 4 nm, exhibited a plateau photocurrent of 2.1 mA cm^{-2}, which is about 60% larger than that for a similar WO_3 photoanode without silver (Figure 4). Also in that case, the photocurrents measured under the back-side 1.5AM solar irradiation were not normalized to take into account the light absorption losses within the TCO substrate.

Significant photocurrent enhancement was also observed under irradiation of the AgNP/WO_3 photoanode from the front side. Notable is also a negative shift by approximately 50 mV of the photocurrent onset potential induced by the presence of underlying silver islands.

The considerable difference between the photocurrent-enhancement factors observed under simulated solar illumination and that corresponding to the IPCEs values suggests an anomalous effect occurring at low incident light intensities. Given the small bandwidth (4 nm) of the monochromator employed for the IPCE measurements, the photocurrents generated, for example, under illumination at 400 nm (where the IPCE of the WO_3 photoanode reaches a maximum) are approximately two orders of magnitude lower than those observed under simulated AM1.5 solar irradiation. We postulate that these small photocurrents generated under low incident light intensities do not allow filling of the electron traps, present within mesoporous WO_3 film, which continue to act as recombination centers. This hypothesis was confirmed by much larger photocurrent-enhancement factors observed in the case of IPCE measurements performed in the solution containing addition of methanol, which is a more efficient hole scavenger than water.

This work confirms the ability of silver Ns to increase the photon-to-current conversion efficiency of a semiconductor photoelectrode operating in aqueous solution. We assign the observed photocurrent enhancement to a combination of optical (nonresonant light scattering and light reflection) and plasmonic (resonant light scattering and electromagnetic field enhancement) effects. In view of the mesoporous nature of the WO_3 film largely penetrated by the electrolyte,[16,17] the portion of the photoactive semiconductor film close to the TCO/AgNP substrate remains within the range of the electromagnetic field generated by irradiated silver particles. This explanation is consistent with the larger IPCE enhancement observed for the AgNP/WO_3 photoanode irradiated with short wavelengths from the back side (see inset of Figure 3 B).

The ability of the silver Ns deposited onto F-doped SnO_2 layer (i.e., TCO/AgNP) to generate strong localized electric fields was confirmed by testing them as SERS (surface-

enhanced Raman scattering) active substrates. We chose benzylidene rhodanine (BR) as a SERS probe molecule as it is expected to exhibit enhancement of a Raman spectrum by increased local electromagnetic field rather than by the charge-transfer effect, as evidenced by a great similarity of the SERS spectrum of BR adsorbed on colloidal Ag to the normal Raman spectrum of solid BR.[19] Intensity of the Raman spectrum collected ex situ for BR adsorbed (after soaking in 1 μM solution of BR for 1 h) on TCO/AgNP is even greater than that obtained for BR adsorbed on a silver colloid (see Figure S3 a,b and description in the Supporting Information).

Further efforts will be directed at optimizing the structure of composite silver/WO_3 films.

Experimental Section

WO_3 films having a thickness of approximately 1 μm were prepared by a sol–gel method based on a tungstic acid/PEG precursor, described in detail elsewhere.[16] Conducting glass plates (Solaronix SA., TCO10-10, 10 Ω/sq) coated with a 0.5 μm thick TCO overlayer of F-doped SnO_2 were used as substrates. The WO_3 films were formed by three consecutive applications of the precursor, followed by annealing in flowing oxygen at 500 °C for 30 min. Silver layers were prepared by sputtering from the Ag target (Johnson Matthey, 99.99 % metal basis) under reduced pressure of 0.07 mbar and a current of 5 mA. The nominal (mass) thickness (2, 3, and 4 nm) of the sputtered layers was estimated from the calibration curve of the Sputter Coater Model SC7620 (Polaron).

The SEM investigations were performed with a Carl Zeiss AURIGA—CrossBeam Workstation. The microscope was equipped with "in lens" SE and ExB detectors and with a bright-field STEM detector.

A Veeco Nanoscope V AFM microscope equipped with a DiMultiMode V scanner was used for imaging the topography of studied samples. Tapping mode AFM (TM-AFM) was employed as it is less destructive towards the surface sample. Cantilevers with a spring constant of 42 $N\,m^{-1}$ and resonance frequency range 311–380 kHz (manufacturer data), tuned prior to further measurement, were applied.

UV/Vis spectra were collected with a double-beam Shimadzu UV-2401 PC spectrophotometer with a 2 nm slit width and 0.2 nm resolution. For both Ag films on TCO and WO_3 samples on TCO/Ag, an uncoated TCO glass slide was used as a reference sample.

Photoelectrochemical experiments were carried out either in 1 M aqueous H_2SO_4 solution (similar results were obtained in 1 M methanesulfonic acid) or in 0.5 M NaCl (acidified to pH 2) using a typical three-electrode setup.

The measurements were carried out in a one-compartment cell equipped with a quartz window, allowing illumination of the WO_3 electrode with minimum optical losses. The exposed surface area of the photoelectrode was 0.28 cm^2. In a typical arrangement, a platinum counter electrode was placed on one side of the working electrode, and the potential of the WO_3 photoanode was monitored vs. mercurous sulfate/mercury reference electrode (MSE) placed on the other side of the working electrode. The WO_3 electrode was polarized anodically at 10 $mV\,s^{-1}$ using a CHI660 Electrochemical Workstation. Simulated AM1.5 solar irradiation was provided by an Oriel 150 W solar simulator fitted with a Schott 113 filter and a neutral density filter.

The wavelength photoresponse (IPCE) of the WO_3 electrodes was measured using a 500 W xenon lamp (Ushio UXL-502HSO) set in an Oriel model 66021 housing and a Multispec 257 monochromator (Oriel) with a bandwidth of 4 nm. The intensity of the incident light from the monochromator was measured by a model 730 A radiometer/photometer (Optronic Lab.)

Raman spectra were collected in the backscattering configuration with a Labram HR800 (Horiba Jobin–Yvon) confocal microscope system equipped with a Peltier-cooled CCD detector (1024 × 256 pixel) using a diode pumped, frequency doubled Nd:YAG laser (532 nm). The confocal pinhole size was set to 200 μm and the holographic grating with 1800 grooves mm^{-1} was used. Calibration of the instrument was performed using a 520 cm^{-1} Raman signal of a silicon wafer. Ex situ SERS spectrum on Ag coated FTO was obtained using a 50 × magnification Olympus objective. For colloidal solution a cuvette holder was used.

Silver colloid was prepared according to procedure described by Creighton et al.,[20] employing $NaBH_4$ as a reducing agent, resulting in particles size ranging from 20 to 30 nm. For SERS measurement, 1 cm^3 of silver colloid was mixed with 10 μL of 10^{-3} M benzylidene rhodanine (BR) ethanolic solution. For SERS measurements on AgNP on TCO, a sample was soaked for 1 h in 10^{-6} M BR solution, prepared by dilution of 10^{-3} M ethanolic solution with water. Ethanolic BR solution and silver colloid were supplied by courtesy of Dr K. Malek (Jagiellonian University).

Received: April 13, 2010
Revised: June 24, 2010
Published online: September 10, 2010

Keywords: nanostructures · photooxidation · silver · water splitting

[1] T. Kume, S. Hayashi, H. Ohkuma, K. Yamamoto, *Jpn. J. Appl. Phys. Part 1* **1995**, *34*, 6448–6451.
[2] O. Stenzel, A. Stendal, K. Voigtsberger, C. von Borczyskowski, *Sol. Energy Mater. Sol. Cells* **1995**, *37*, 337–348.
[3] R. H. Ritchie, *Surf. Sci.* **1973**, *34*, 1–19.
[4] C. F. Bohren, D. R. Huffman, *Absorption and Scattering of Light by Small Particles*, Wiley-Interscience, New York, **1983**.
[5] H. A. Atwater, A. Polman, *Nat. Mater.* **2010**, *9*, 205–213.
[6] S. Pillai, K. R. Catchpole, T. Trupke, M. A. Green, *J. Appl. Phys.* **2007**, *101*, 093105.
[7] D. Derkacs, S. H. Lim, P. Matheu, W. Mar, E. T. Yu, *Appl. Phys. Lett.* **2006**, *89*, 093103.
[8] A. Morfa, K. Rowlen, T. Reilly, M. Romero, J. van de Lagemaat, *Appl. Phys. Lett.* **2008**, *92*, 013504.
[9] T. Reilly, J. van de Lagemaat, R. Tenent, A. Morfa, K. Rowlen, *Appl. Phys. Lett.* **2008**, *92*, 243304.
[10] S.-S. Kim, S.-I. Na, J. Jo, D.-Y. Kim, Y.-C. Nah, *Appl. Phys. Lett.* **2008**, *93*, 073307.
[11] J.-Y. Lee, S. T. Connor, Y. Cui, P. Peumans, *Nano Lett.* **2010**, *10*, 1276–1279.
[12] S. D. Standridge, G. C. Schatz, J. T. Hupp, *J. Am. Chem. Soc.* **2009**, *131*, 8407–8409.
[13] M. A. Butler, *J. Appl. Phys.* **1977**, *48*, 1914–1920.
[14] M. Spichiger-Ulmann, J. Augustynski, *J. Appl. Phys.* **1983**, *54*, 6061–6064.
[15] C. Santato, M. Ulmann, J. Augustynski, *Adv. Mater.* **2001**, *13*, 511–514.
[16] C. Santato, M. Odziemkowski, M. Ulmann, J. Augustynski, *J. Am. Chem. Soc.* **2001**, *123*, 10639–10649.
[17] B. D. Alexander, P. J. Kulesza, I. Rutkowska, R. Solarska, J. Augustynski, *J. Mater. Chem.* **2008**, *18*, 2298–2303.
[18] J. J. Ruiz-Perez, J. M. Gonzalez-Leal, D. A. Minkov, E. Marquez, *J. Phys. D* **2001**, *34*, 2489–2496.
[19] K. Malek, Jagiellonian University, personal communication.
[20] J. A. Creighton, C. G. Blatchford, M. G. Albrecht, *J. Chem. Soc., Faraday Trans. 2* **1979**, *75*, 790–798.

